11

Morphologies of Polymer Crystals in Thin Films

Günter Reiter[1], Ioan Botiz[1], Laetitia Graveleau[1], Nikolay Grozev[1], Krystyna Albrecht[2], Ahmed Mourran[2], and Martin Möller[2]

[1] Institut de Chimie des Surfaces et Interfaces, ICSI-CNRS, 15, rue Jean Starcky, B.P. 2488, 68057 Mulhouse Cedex, France
[2] DWI an der RWTH Aachen, Pauwelsstr. 8, 52056 Aachen, Germany
g.reiter@uha.fr

Abstract. We present microscopy investigations on the morphology of crystals of poly-2-vinylpyridine-polyethyleneoxid diblock copolymers ($P_2VP - PEO$) in thin films with thicknesses below and above the thickness of a single lamella. For crystallisation temperatures above 45°C, nucleation is highly unlikely. Thus, the resulting morphologies represent essentially single crystals, allowing us to relate morphology to the kinetics of crystal growth. In several examples we demonstrate the influence of thermal history and film thickness on molecular orientation and pattern formation during crystal growth. We discuss the analogies and differences between crystallisation of small molecules and polymers.

11.1 Introduction

The extraordinary beauty and the vast diversity of the possible morphologies represents one of the main reasons why crystallization attracts our interest. Of course, many properties (mechanical, optical, electrical, ...) depend on the detailed structure of crystalline materials. Thus, it is highly important to understand how crystals grow and how the various morphologies result from growth processes which can be controlled via parameters like temperature or concentration.

At first glance, forming a crystal starting from individual molecules seems to be an easy task. One simply has to assemble these molecules according to the "construction manual" defined by the characteristic parameters of the unit cell of the crystal. However, if the crystallization process advances at a finite growth rate, complications arise due to the necessary transport of the molecules towards the "construction site" and the time needed for the integration into the crystal. As a consequence, the growth front becomes unstable and the resulting crystals are less perfect in the sense that their morphology is not any longer exhibiting the rather simple form of the unit cell. Fascinating patterns are created as can be seen frequently in Nature, for example in

G. Reiter et al.: *Morphologies of Polymer Crystals in Thin Films*, Lect. Notes Phys. **714**, 179–200 (2007)
DOI 10.1007/3-540-47307-6_11

snowflakes [1]. Such instabilities of the growth front can be reduced in frequency, or eliminated completely, if the growth process proceeds at low rates. Then, each molecule arriving at the front will have enough time to "examine" the crystal surface and to find the "ideal" location for its integration in the crystal. "Ideal" means that the growth front stays smooth as in such case each molecule will profit from having the maximum possible number of neighbouring molecules, thereby reducing the free energy of the system. This reflects the fact that the most stable state of a crystal is exhibiting well-defined facets which one can observe even on macroscopic scales. The two key processes which determine if growth is sufficiently slow to allow for the formation of ideal crystals are:

- The transport of the molecules to the crystal. In order to build a crystal, enough molecules have to be available at the growth front. Transport can be controlled by the concentration of molecules in solution or by their rate of diffusion.
- The probability to attach a molecule at a crystal surface. This probability should not be equal to unity as this would mean that the molecules are fixed at the place of the crystal where they arrive first. This would not allow for the elimination of defects like cavities, as almost no molecules will be able to diffuse into "fjord-like" channels.

The attachment probability can be influenced by several parameters. For example, one can control the attachment probability and consequently the growth rate via temperature. Crystallization is only possible below the melting point of the system. Exactly at the melting temperature, the probability for attaching a molecule to the crystal is so low that the molecule will not stay attached. Thus, the crystal will not grow. Attachment may also be in competition with the displacement of other molecules like solvent molecules, additives or impurities. For example, if an additive is strongly adsorbed onto the crystal surface the crystal will not grow as fast as in cases when these additional molecules are not present.

If the probability of attachment is high (low chance of desorbing molecules from a crystal), crystal growth is dominated by diffusion of the molecules to the crystal front. In this so-called "diffusion limited aggregation" (DLA) regime [2–14] the resulting complex patterns (e.g. "tree-like", dendritic,...) can be characterized according to their morphology and their average density upon increasing size [4]. This density, while being less than the density of an "ideal" faceted crystal, may either be constant (= compact) or decreasing as one moves away from the nucleation site (= fractal).

In the absence of anisotropy of the attachment probability for the various crystal faces, in the absence of anisotropic diffusion or without any selective influence of additives, random growth will be the result, exhibiting no preferred overall directions. Locally, however, the characteristic parameters of the unit cell (like the characteristic angles between the crystal axes) will be respected, which may also be visible on macroscopic scale, for example via a

six-fold symmetry of the resulting fractal pattern (compare snowflakes [1] or for thin films of isotactic polystyrene [10, 11, 15]).

It should be noted that all non-ideal, kinetically controlled structures like snowflakes represent out-of-equilibrium objects. That means that they depend on the conditions under which they were formed and also on how they evolved in time after growth (history dependence). Qualitatively, one may state that the faster the patterns were formed, the more they consist of small subunits (thinner branches or smaller objects constituting the pattern [6–8]), the more fragile they are and the more they tend to change with time ("ageing effect") [16, 17].

All the aspects and processes discussed above apply also to the crystallisation of polymers [18–31]. However, in addition, the connectivity of the monomers causes several restrictions. One of the most obvious ones is represented by the quasi-two-dimensional lamellar shape of polymer crystals. A lamella is formed by crystalline segments of the chain (the stems) arranged vertically and limited (on top and below) by amorphous (fold) surfaces. Therefore, polymer crystals grow essentially only in two dimensions. Growth in the third dimension is rather difficult, in particular when the polymer contains non-crystallisable units which will segregate to the surfaces of the crystals. Growth in the third dimension necessitates deviations from the perfect lamellar structure, e.g. screw dislocations. The topic of polymer crystallisation has been the subject of a tremendous amount of studies over the last 60 years [5–8, 10–65].

In the here presented experimental study of crystal growth and morphology development we will control the number of available molecules by using thin films of varying thickness [12]. Thickness also affects the transport process as a thickness-dependent depletion zone forms between crystal front and molten film. The attachment probability will be mainly controlled by the crystallization temperature. Finally, the growth rate depends on both, film thickness and temperature. We mainly focus on the formation of mono-lamellar single crystals. By using block copolymers with one amorphous block, we take advantage of the additional confinement effect imposed by the rather thick glassy layers on the surfaces of the lamellae formed by the amorphous block. Moreover, we have chosen a polymer where the amorphous block also is responsible, in comparison to the corresponding crystallisable homopolymer, for lowering the probability of nucleation. Thus, by effectively suppressing nucleation, we can clearly distinguish between nucleation events and growth processes. We aim at understanding how the various morphologies observed in such thin polymer films can be related to growth processes. In addition, we also try to identify patterns where the polymer aspects become evident or even dominant.

11.2 Experimental Section

Thin Films of P_2VP-PEO Diblock Copolymers

For our studies we used a poly-2-vinylpyridine-polyethyleneoxid block copolymer ($P_2VP-PEO$, $M_w = 16400 + 46600$ g/mol, $M_w/M_n < 1.14$) which was synthesized in the group of Martin Möller.

The crystallizable block is polyethyleneoxide, a well investigated polymer [6, 7, 12, 23, 59]. Various studies have also been performed with block copolymers [32, 40–42]. The maximum length of the crystalline PEO block in the fully extended state is: $L = l_u N = 295$ nm with $l_u = 0.2783$ nm [22] and $N = 1060$ is the number of monomers.

Samples were prepared from dilute toluene solutions by spincoating thin films onto the wafers. The polymer adsorbed onto the oxide surface of silicon wafers which were cleaned in a water-saturated UV-ozone atmosphere. By this cleaning procedure, we created a surface with a high density of hydroxyl groups. The initial film thickness has been determined by ellipsometry. Crystallization and subsequent thermal treatment (annealing) were performed directly under an optical microscope in an inert atmosphere (nitrogen flow).

Online inspection of the crystallization process by optical microscopy was used to determine the growth rates. Atomic force microscopy (AFM), a technique often employed for the investigation of polymer crystallization (see for example: [12, 16, 37, 38, 48, 51–58, 60–65]), was used to visualize the resulting crystal morphology in more detail.

Optical Microscopy Measurements

The samples were placed onto an enclosed hotplate, purged with nitrogen, under a Leitz-Metallux 3 or an Olympus BX51 optical microscope. The crystallisation temperature at the hot stage was controlled to within 0.1 degrees. No polarization or phase contrast was used. Contrast is due to the interference of the reflected white light at the substrate/film and film/air interface, resulting in well-defined interference colours which could be calibrated with a resolution of about 10 nanometers. This is sufficient to allow to visualize the growth of crystalline structures even in monolayer regions. For the thicker films around 100 nm (light blue interference colour) studied in this work, the interference patterns became the lighter the thicker the films (or crystals) were. For films around 20-40 nm (brown interference colour), the interference patterns became the darker the thicker the films (or crystals) were. We have followed the progression of the crystal growth front in real time by capturing images by a CCD camera. It should be noted that in all of the thin films studied here, only very few nucleation sites have been observed on the whole sample. At temperatures above about 45°C, no nucleations events were observed for many hours (after cooling down from higher temperatures). In order to allow nonetheless for crystallisation at such high temperatures, the sample

was either shortly cooled to lower temperatures or a sort of self-seeding was employed by melting a sample, which was first crystallized at rather low temperatures like room temperature, at temperatures around 65°C for about 1 to 2 minutes and then lowering the temperature to the chosen crystallisation temperature. Experiments at temperatures above about 45°C allowed us to follow the progression of the crystallisation front of single crystals over distances of many 100 micrometers without the interference with any nucleation events.

Atomic Force Microscopy (AFM)

Measurements were performed with a Nanoscope IIIa/ Dimension 3000 (Digital Instruments) in the tapping mode at ambient conditions, using the electronic extender module allowing simultaneously the phase detection and height imaging. We used Si-tips (model TESP) with a resonant frequency of about 160–190 kHz. Scan-rates were between 0.2 and 4 Hz. The free oscillation amplitude of the oscillating cantilever was typically around 50 nm, the setpoint amplitude (damped amplitude, when the tip was in intermittent contact) was slightly lower. Topographic (height mode) and viscoelastic (phase-mode) data were recorded simultaneously.

11.3 Results and Discussion

11.3.1 Changes in Morphology with Crystallization Temperature

It is of course well-known that the morphology of a crystal depends in an clearly visible way on the crystallisation temperature, or more precisely the degree of undercooling. Primarily, this is caused by the temperature dependant rate at which molecules get attached and integrated into a crystalline structure. The slower this rate, the "simpler" are the crystalline structures in terms of morphology. However, we want to emphasize that even crystals of rather complex morphology like dendrites may still be single crystals where all molecules are perfectly ordered with respect to each other.

We investigated crystallization of polymers by following the process in real time under a microscope. In a first approach, we have chosen films of thickness significantly larger than the thickness of one lamella. In Fig. 11.1, a typical result, reminiscent of spherulitic growth, is shown.

At a crystallization temperature (T_c) of 45°C, growth is isotropic in all directions, expressed by a constant radial growth rate of 8.85 μm/min. We note that the orientations of the characteristic features ("fingers") are fluctuating randomly around the radial direction. Although the pattern (see Fig. 11.1C) clearly indicates the competition between the individual fingers, none of these fingers is able to "run away" from all others. At a scale larger than the size of the fingers, the growth front is comparatively smooth. Ahead of this front, a

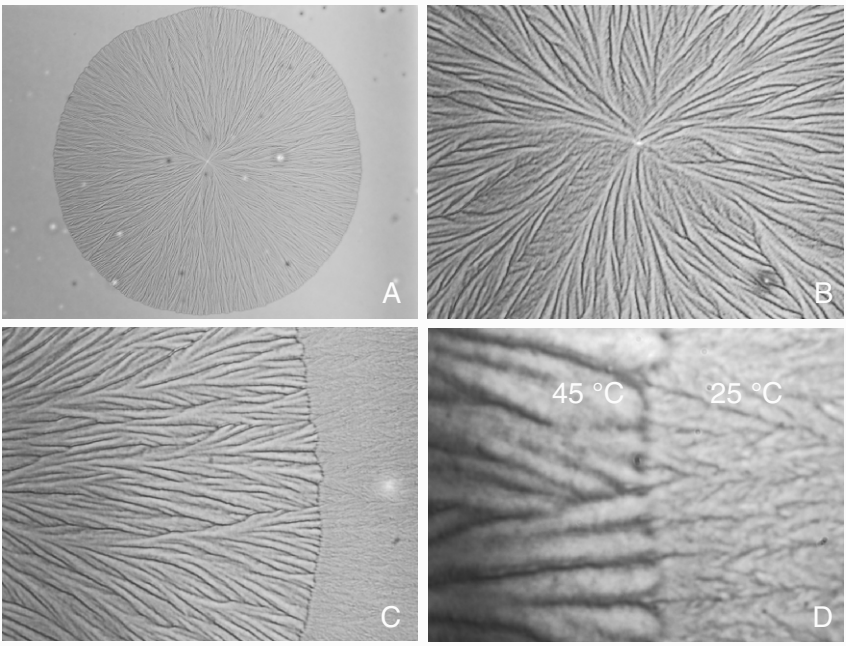

Fig. 11.1. Typical micrographs obtained for crystallization in a 108 nm thick film, taken after growing the crystal for 130 min at 45°C at a radial growth rate of 8.85 μm/min and then quenching the sample to room temperature. The images have the following sizes: (**A**) 865×650 μm^2, (**B**) +(**C**) 174×131 μm^2, and (**D**) 35×26 μm^2

depletion zone can be observed, particularly visible in the higher resolution of Fig. 11.1D. The finer fingers in the right part of Fig. 11.1D result from faster growth at room temperature. At this thickness the lighter parts (light blue, resulting from interference of white light) are thicker than the darker (dark blue) ones.

At the higher temperature of Fig. 11.2 ($T_c = 50$°C), and in contrast to Fig. 11.1, growth is not isotropic but is clearly "guided" by four orthogonal directions. Perpendicular to these main axis, side branches are formed, from which several generations of always orthogonal branches depart. It is interesting that the hierarchy of side-branches leads to rather smooth lateral faces building the frontiers of square-shaped single-crystal. It should be noted that the thickness of the diagonals is slightly higher than that of all side-branches. The tips of the diagonals can be considered as the driving points of crystallization in this system. As in Fig. 11.1, we can clearly observe a depletion zone ahead of the crystal front. Interestingly, at lengthscales significantly larger than the width of the individual branches, these side-branches seem to create

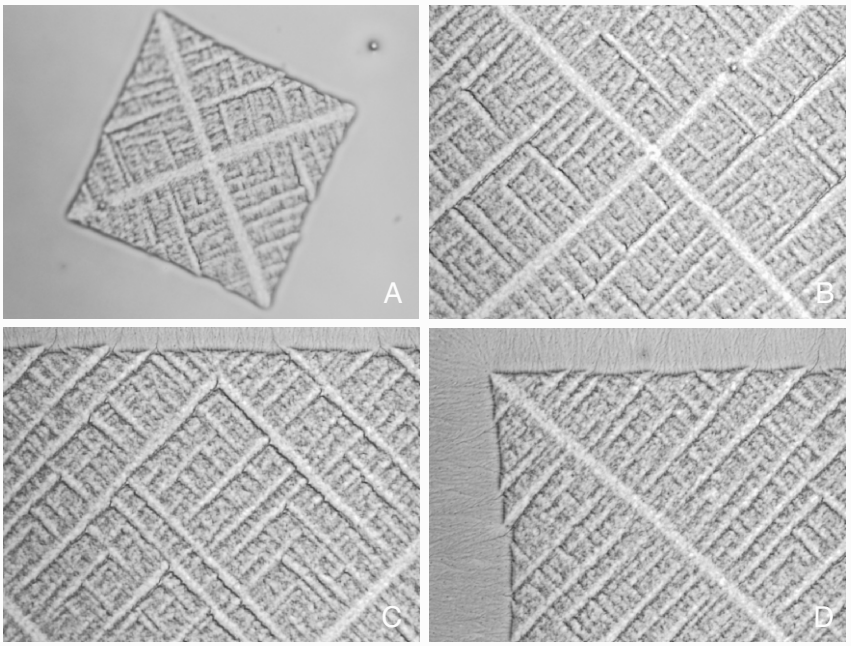

Fig. 11.2. Typical micrographs obtained for crystallization in a 108 nm thick film. Image (**A**) was taken at the beginning of crystallization while images (**B**)–(**D**) were taken after growing the crystal for 160 min at 50°C at a rate of 3.88 μm/min (along the diagonal) and then quenching the sample to room temperature. The size of all images is: 174×131 μm^2. At this thickness the lighter parts (*light blue*) are thicker than the darker (*dark blue*) ones

a super-structure via the alternating dominance of every fifth or so orthogonal side-branch of the same generation.

We note that such a transition from a circular to a quadratic envelope of the crystals has also been reproduced by computer simulations [13,14]. There, this transition is due to the reduction of the growth front nucleation probability. While the disk-like pattern consists of multiple crystals, the square-shaped pattern represents a single crystal. We thus assume that, for the given film thickness, we observed a transition from a polycrystalline structure to a single crystal within the temperature interval from 45 to 50°C.

When increasing the temperature to $T_c = 55$°C (Fig. 11.3), growth proceeded similar to Fig. 11.2. This can be seen from the dominance of the diagonals. However, the hierarchy of side-branches is less visible because there are fewer but wider side-branches and the gaps between them have been almost completely filled. This was possible as, at such slow growth, transport was not the limiting step. In addition, as more perfect crystals could be formed, the probability for the nucleation of screw dislocations was reduced. It should be

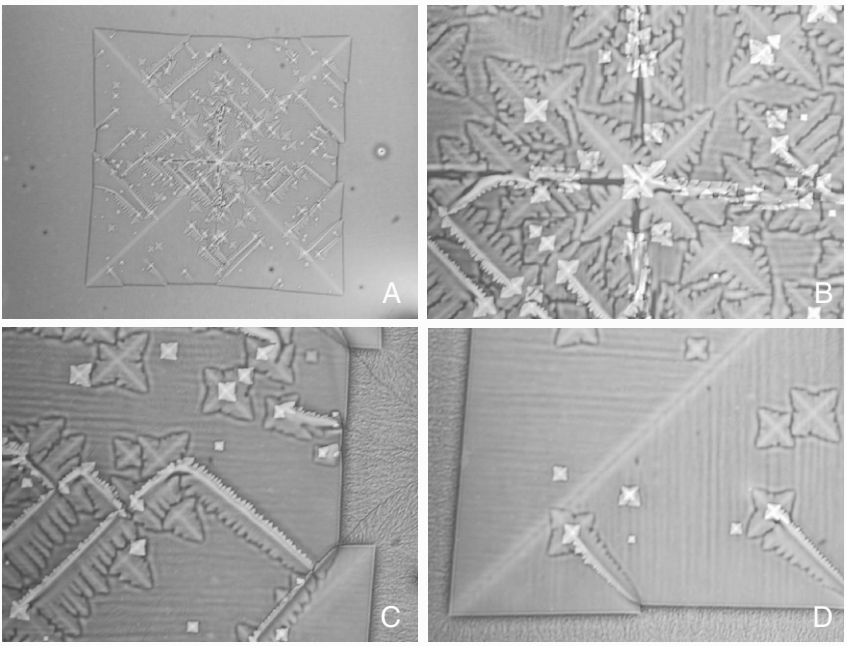

Fig. 11.3. Typical micrographs obtained for crystallization in a 108 nm thick film, taken after growing the crystal for 855 min at 55°C at a rate of about 1 μm/min (along the diagonal) and then quenching the sample to room temperature. The images have the following sizes: (**A**) 865×650 μm^2, (**B**)–(**D**) 174×131 μm^2. At this thickness the lighter parts (*light blue*) are thicker than the darker (*dark blue*) ones

realized that a 108 nm thick film is thicker than one lamella and thus much more molecules than needed for the formation of a completely filled lamella are available. We also want to draw the attention to the undulations (ripples) clearly seen in Fig. 11.3D, which form parallel lines at an angle of 45 degrees to the leading diagonal. The spacing between these ripples is highly constant. In addition, these ripples are not perturbed by spirals which most likely resulted from dislocations originating at the junction line between side-branches. Thus, we may conclude that these ripples can cross several side-branches. This may indicate that the ripples are not necessarily originating from the crystal and need not to be crystalline either.

11.3.2 Dependence of Morphology on Initial Film Thickness

Looking at Fig. 11.4, it is certainly intriguing to note that the same kind of square shaped envelope as in Figs. 11.2 and 11.3 is also observed for much thinner films, even thinner than the height of the lamella. (Depending on crystallisation temperature, the lamella thickness varied between about 20 nm

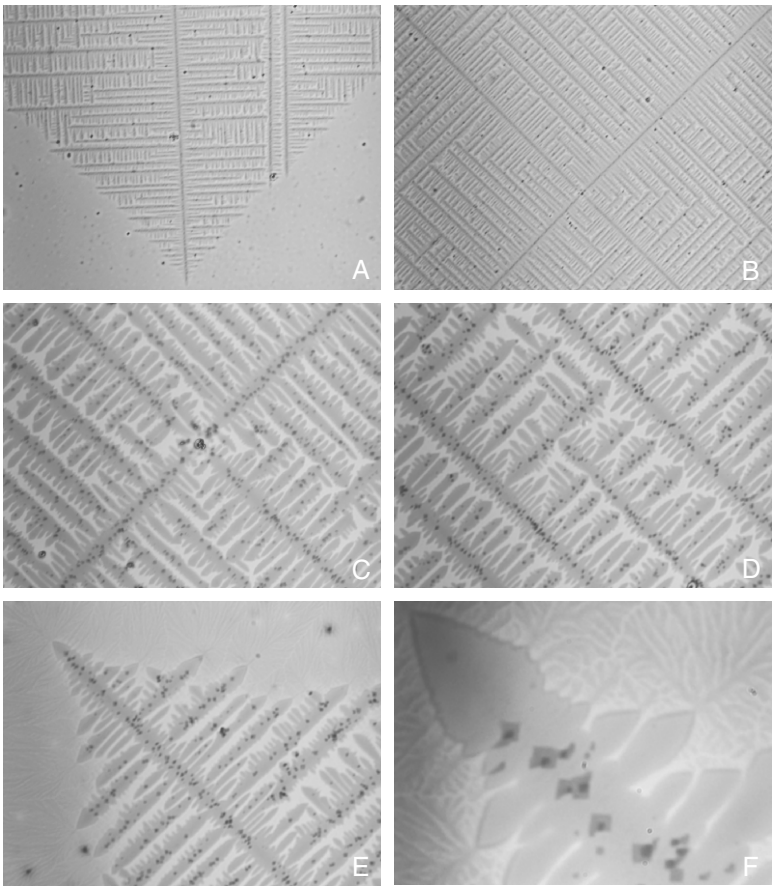

Fig. 11.4. Typical micrographs obtained for crystallization in a 37 nm thick film, taken after growing the crystal for 16 hours at 50°C at a rate of 0.7 μm/min (along the diagonal) and then quenching the sample to room temperature. The images have the following sizes: (**A**) and (**B**) 865×650 μm^2, (**C**)–(**E**) 174×131 μm^2, and (**F**) 35×26 μm^2. At this thickness the darker parts (*brown*) are thicker than the lighter ones

for $T_c = 25$°C and about 45 nm for $T_c = 55$°C, as measured by AFM). Moreover, the dendritic structure does not differ qualitatively for thick and thin films. However, for the thin film a clear depletion zone, exposing even the substrate, can be seen in between the individual branches. Therefore, we can easily distinguish the multiple generations of side branches, all mutually orthogonal to each other.

When using thicker films (see Fig. 11.5), we qualitatively can find many similarities to the previous Figs. 11.2 to 11.4. The conditions (film thickness and crystallisation temperature) are similar to Fig. 11.3. However, this sample

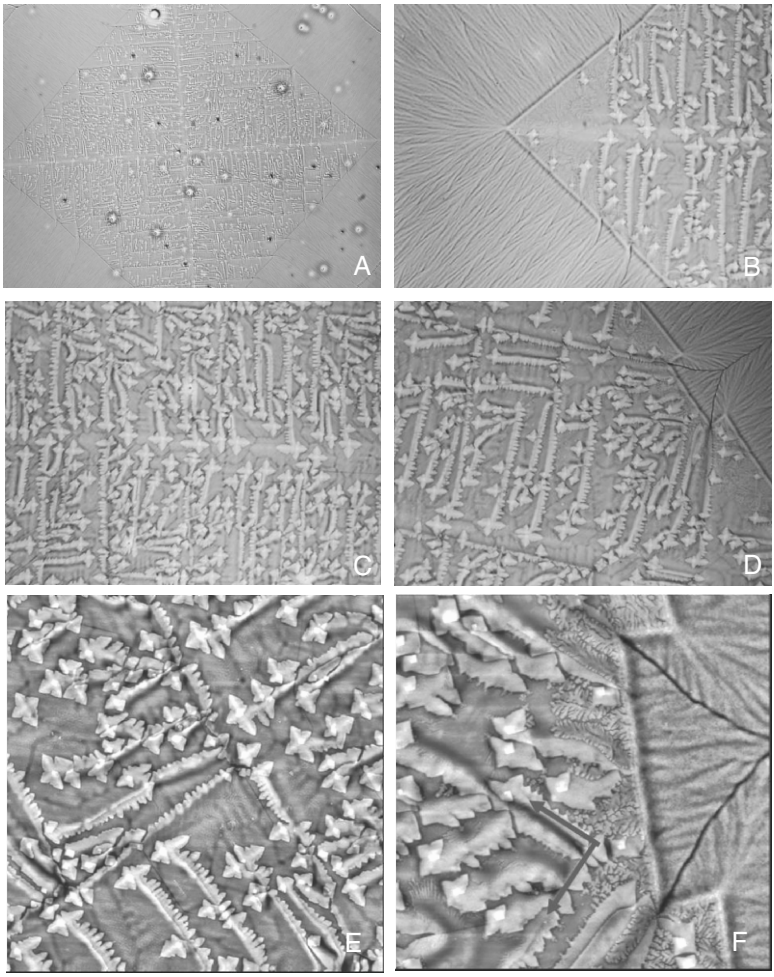

Fig. 11.5. Optical micrographs (**A**–**D**) and AFM images (**E**–**F**) obtained for crystallization in a 97 nm thick film, taken after growing the crystal for 893 min at 55°C at a rate of about 0.7 μm/min (along the diagonal) and then quenching the sample to room temperature. The images have the following sizes: A) $865 \times 650\ \mu m^2$, (**B**)–(**D**) $174 \times 131\ \mu m^2$, (**E**) $70 \times 70\ \mu m^2$, and (**F**) $40 \times 40\ \mu m^2$. At this thickness the lighter parts in A–D (*light blue*) are thicker than the darker (*dark blue*) ones

showed for an unknown reason a stronger tendency for spiral formation. Thus, the underlying dendritic pattern got nicely decorated with spirals. The interesting point is that due to the square-like geometry of the spirals we are able to conclude that all these spirals are uniformly oriented, in clear registry with the underlying morphology of the orthogonal branches. The diagonal of the square-like spirals are parallel to the diagonals of the underlying large

square-shaped crystal. We can also deduce that the spirals are mainly (if not exclusively) formed at junction lines between branches. The key features (diagonals, distance between branches, ...) can be easily anticipated from the arrangement of the spirals. We also can identify the importance of the tips of the branches and the crystal-melt interfaces (CMI) with respect to the growth process. This becomes obvious when analysing these regions after a temperature jump to room temperature (see Figs. 11.5D and 11.5F). There, the finer branched patterns originating from crystallisation at room temperature depart in both directions. On top of the crystalline structure grown at 55°C, these branches grew away from the CMI in the direction opposite to the growth direction at 55°C. In addition, crystalline structures depart also in the other direction away from the CMI.

Growing polymer crystals in films significantly thinner than the lamella and at temperatures close to the melting point leads to rather compact crystals as shown in Fig. 11.6. We emphasize that under such conditions crystals only grow very slowly, allowing the perfecting of the crystals. Therefore, the width of the side branches is becoming significantly larger and only few side-branches are formed. It may be anticipated that the same pattern as in Fig. 11.4 could be observed if the crystals grew up to macroscopic sizes of centimetres.

We also want to draw the attention to the undulations (or ripples) visible at the surface, comparable to the ones seen in Fig. 11.3. In agreement with the observations of [15], the distance between these ripples depends on crystallisation temperature. We point out again that these ripples are at an angle of 45 degrees to the main growth direction represented by the diagonals. At the same time, the ripples are orthogonal to the faces of the square-like envelope of the crystal. We note that such ripples are not only seen in the square-shaped crystals of PEO but similar observations have been made also for the hexagonal crystals of isotactic polystyrene [10, 11, 15].

Although the sample shown in Fig. 11.7 was crystallized under almost the same conditions as the one in Fig. 11.6, the fact that it could grow at a higher rate (due to the higher number of available molecules – the film was about 11 nm thicker – the crystal front moved faster) the crystal front is more prone to become unstable. Therefore, the square-shape envelope of the crystal is not established. Nonetheless, some features like the four-fold symmetry and the dominance of the diagonals are reproduced also in this situation. The ripples are also clearly visible.

After cooling down the sample to room temperature the sample crystallized at a much faster rate and thus we observe much finer patterns. At the crystal front flat-on oriented lamellae were formed, reflecting also the orientation of the crystal formed at 55°C. Interestingly, while the flat-on oriented lamellae originating from the tip survived, the ones further away from the tip were stopped by the arrival of apparently faster growing edge-on lamellae. This competition (simultaneous appearance) of flat-on and edge-on lamellae exists also at the boundaries of the crystal shown in Figs. 11.6B and 11.6C.

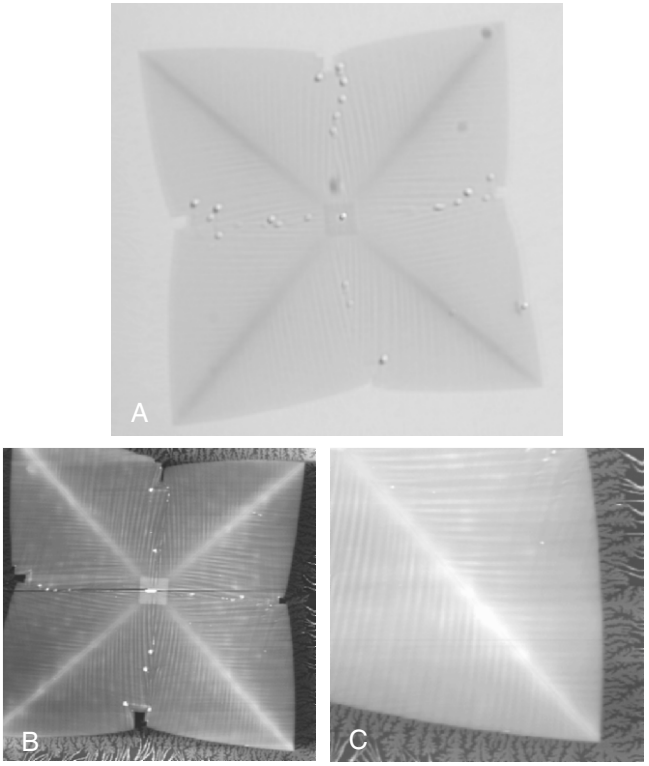

Fig. 11.6. Typical optical micrograph (**A**) and AFM height images (**B** and **C**) obtained for crystallization in a 26 nm thick film, taken after growing the crystal for 2300 min at 55°C at a rate of about 0.045 μm/min (along the diagonal) and then quenching the sample to room temperature. The images have the following sizes: (A) 90×86 μm^2, (B) 75×75 μm^2, with a height range of 120 nm, and (C) 38×38 μm^2, with a height range of 70 nm. At this thickness the darker parts (*brown*) in (A) are thicker than the lighter ones

11.3.3 The Kinetics of Crystal Growth and the Effect of Changing Temperature

In order to visualize how dendritic crystals grow and how a square-shape envelope is formed from such dendritic structures, we have superposed two images from the same crystal taken at an interval of 95 sec (see Fig. 11.8). As we want to focus on single crystals only, we have chosen a rather thin film of about 40 nm in order to avoid growth front nucleation (GFN) [13, 14]. GFN depends on the number of molecules present. Thus, in such thin films the transition from poly-crystals to single crystals can occur at lower temperatures than in the 108 nm thick films discussed above.

In the centre of Fig. 11.8, we can clearly identify the square consisting of a dentrictic structure of comparatively small side-branches, resulting from

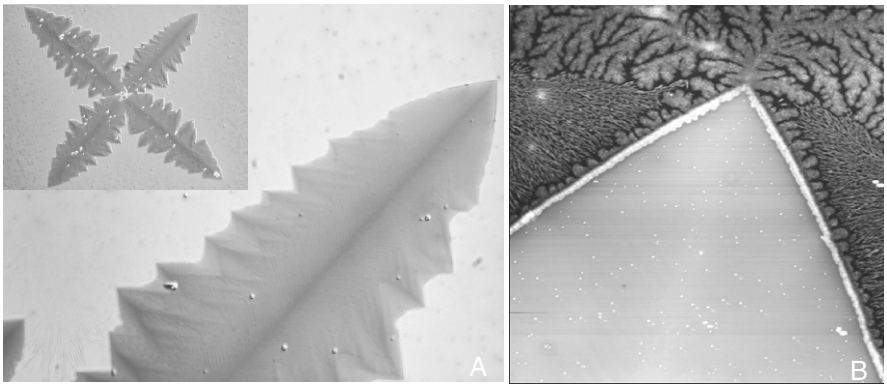

Fig. 11.7. Typical optical micrograph (**A**) and AFM image (**B**) obtained for crystallization in a 37 nm thick film, taken after growing the crystal for 2300 min at 55°C at a rate of about 0.2 μm/min and then quenching the sample to room temperature. The images have the following sizes: (A) 174×131 μm^2 (the size of the inset is: 500×377 μm^2) and (B) 25×25 μm^2, with a height range of 100 nm. At this thickness the darker parts (brown) in (A) are thicker than the lighter ones

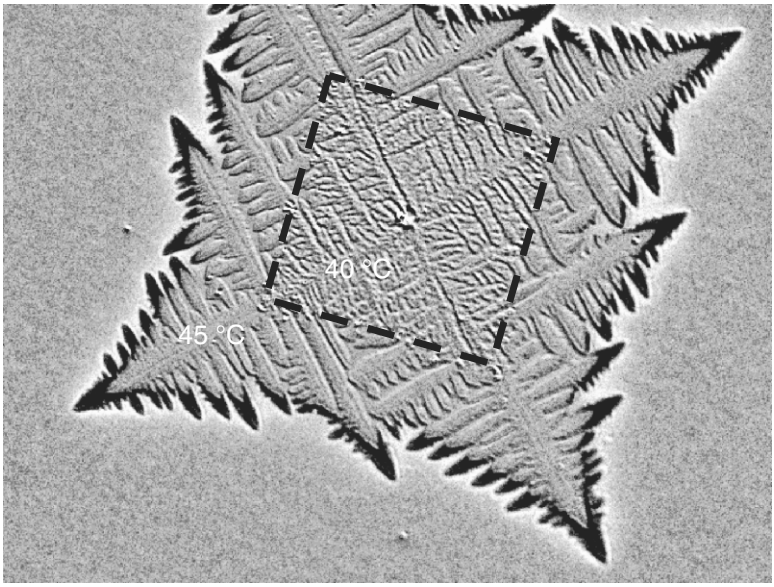

Fig. 11.8. Superposition of two optical micrographs taken at an interval of 95 sec for a 40 nm thick film. For the first image, the sample was first kept at 40°C for 300 seconds and then for 480 seconds at 45°C. The difference between the two images, i.e. the distance the crystal grew, is represented in black. The size of the image is 174×131 μm^2

crystallisation at 40°C at a rate of about 7.3μm/min. The outer part was grown at 45°C at a rate of about 5.5μm/min.

The superposition of two images at an interval of 95 sec allows to clearly identify the points where the crystal grew. Growth proceeded mostly via the primary tips along the diagonals and some of the major side branches. Secondary branches were much less contributing. We also note that the structures are not fully symmetric, neither around one individual diagonal nor when comparing the detailed structures of "trees" along different diagonals. We can conclude from this figure that the envelope of the crystals can only be approximated by a straight line if the number of dominant side-branches is large.

We have already mentioned several times before that faster growing crystals exhibit a higher frequency of side-branching. In Fig. 11.9, we present such a transition from small to wide side-branches in a single experiment by applying a temperature jump from 50°C to 55°C. It can be clearly seen that at the lower temperature four main "dendritic trees" are growing in orthogonal directions. At such conditions, the envelope is rather quadratic. We want to draw the attention also to the junction lines where the trees meet, which are at an angle of 45 degrees to the diagonals of the square. However, after raising the temperature, the number of side-branches is significantly reduced (on the average about 4 branches are fused to one). It may be anticipated that also at this higher crystallization temperature, after appropriate rescaling of the image size, the same qualitative quadratic shape of the crystal would be obtained but after significantly longer crystallization time.

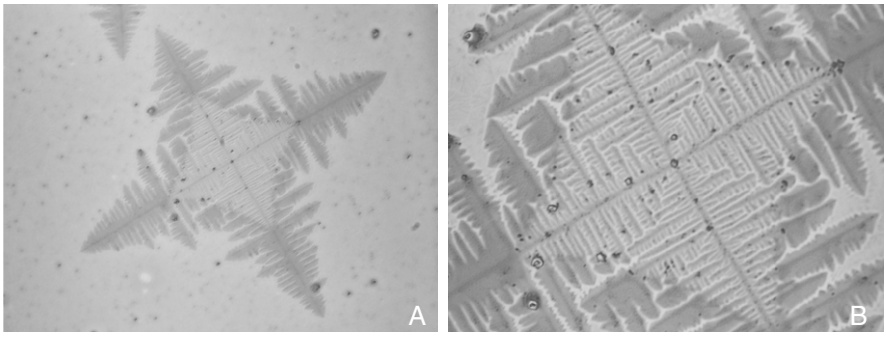

Fig. 11.9. Optical micrographs of a crystal in an about 32 nm thick film which grew first for 24 hours at 50°C and then for 72 hours at 55°C before the sample was cooled to room temperature. The size of the images is (**A**) 430×235 μm^2, (**B**) 174×131 μm^2

11.3.4 "Decoration" of Flat-On Lamellar Crystals by Ripples and Spirals

Optical microscopy allows to follow crystal growth in real time. Due to the interference effect, which is the advantage of reflecting substrates such as silicon wafers, we can demonstrate that the ripples were formed *during* growth and are not, for example, the consequence of a mechanical instability induced by a temperature jump. In Fig. 11.10, it can been seen that these ripples existed already during growth at 57°C, and were continuously formed as the crystals grew. While the ripples are perpendicular to the (lateral) sides of the squares, the spirals, once nucleated at the growth front, form tails at an angle of 45 degrees. It is highly probable that the spirals, and the subsequent tails, formed at the junction line between two underlying side-branches. This is consistent with our conclusions drawn in the context of Fig. 11.3.

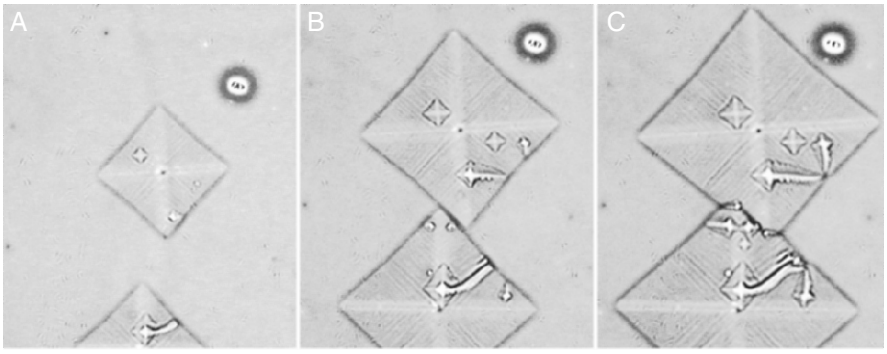

Fig. 11.10. Series of three optical micrographs taken at an interval of (**B**) 69 min and (**C**) 114 min for a 102 nm thick film during crystallization at 57°C. The size of the images is 35×41 μm^2

From Fig. 11.11, we can conclude, taking advantage of the square-shaped spirals, that *all* spirals are oriented along the underlying individual branches. *All* spirals have exactly the same orientation of their diagonals as the dendrites seen in the optical micrograph. Thus, it is not surprising that all spirals are correlated among themselves, as can be nicely seen in Figs. 11.11C and 11.11D.

The process of spiral formation can be deduced from details observed by AFM, as shown in Fig. 11.12. A film of 102 nm is more than twice as thick as one lamellar thickness (about 45 nm at 57°C). Thus, the first lamella, growing close to the substrate is still covered with a large reservoir of non-crystalline – but crystallizable – polymers. From our experiments, it turned out that the junction lines between side branches are regions of high probability for spiral nucleation. These spirals may either form a new lamella, similar in shape as the underlying square-shaped lamella (see Figs. 11.10 and 11.12A). Or, as shown in Figs. 11.10 and 11.12C, such spirals may be accompanied by a

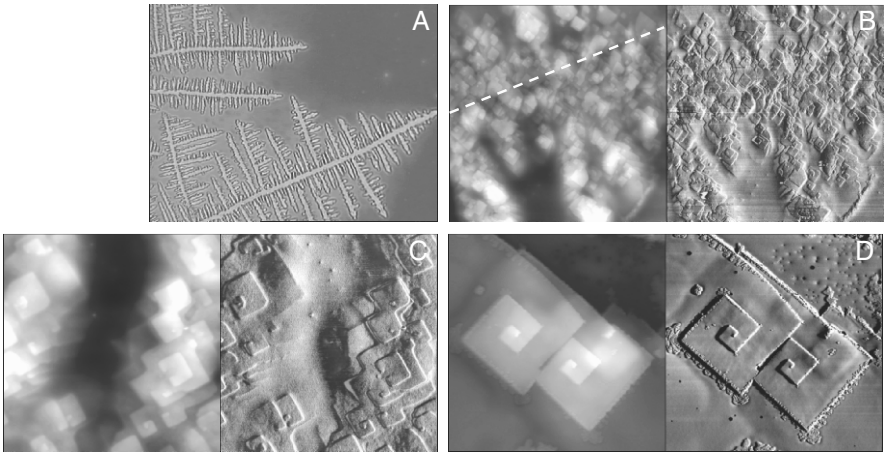

Fig. 11.11. (**A**): Optical micrograph of an about 70 nm thick film taken after growing the crystal for 66 hours at 40°C and then quenching the sample to room temperature. (**B**) and (**C**): AFM images (*left*: topography and *right*: phase) of the same crystal. (**D**): AFM image (left:topography and right: phase) of spirals formed in a 50 nm thick film, crystallized for 72 hours at 55°C. The size of the images is (A) $290 \times 218\ \mu m^2$, (B) $15 \times 15\ \mu m^2$, (C) $5.5 \times 5.5\ \mu m^2$, (D) $15 \times 15\ \mu m^2$

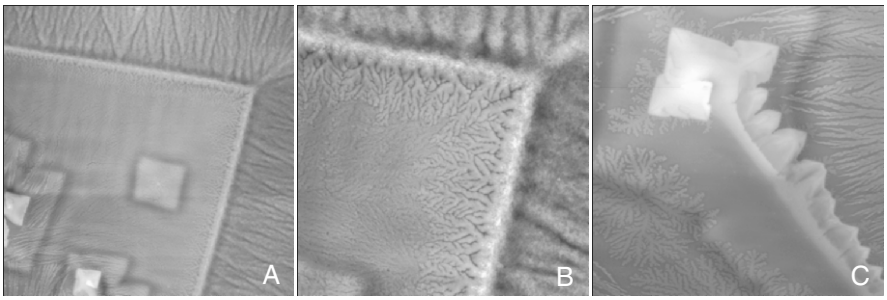

Fig. 11.12. AFM images showing some details on spirals and "secondary" crystalline structures formed on top of a crystal for a 102 nm thick film crystallized at 57°C and then quenched to room temperature. Besides the spirals which grew at 57°C, we also can identify crystals grown at room temperature. The size of the images is (**A**) $50 \times 50\ \mu m^2$ (height range: 150 nm), (**B**) $20 \times 20\ \mu m^2$ (height range: 80 nm), (**C**) $20 \times 20\ \mu m^2$ (height range: 180 nm)

tail which most likely "decorates" the junction line between side-branches. The basic mechanism for why such junction lines represent locations of high probability for spiral nucleation is not yet clear. Interestingly, the growth fronts also present locations of high nucleation probability as can be seen in Fig. 11.12B (see also Fig. 11.5). There, after cooling the sample to room temperature, many flat-on lamellae depart in both directions, backwards and forwards.

11.3.5 Orientation of the Crystalline Lamellae with Respect to the Substrate

As a final remark, we would like to mention that the orientation of the lamellae is not necessarily parallel to the substrate. Actually, as already indicated in Figs. 11.6 and 11.7 for thin films, both orientations of the lamellae can occur simultaneously. Interestingly, also for thicker films, Figs. 11.13 and 11.14 indicate that while at low temperatures most likely edge-on lamellae are formed, flat-on structures are more favourable at higher temperatures. The wedge-like structure seen in optical microscopy can be identified as flat-on lamellae. The fact that such wedges are widening demonstrates that the growth rate of flat-on structures at the higher crystallisation temperatures is slightly higher than the one of the edge-on lamellae. Thus, after sufficiently long time, and assuming that nucleation is not the dominating process, only flat-on lamellae continue to grow. In Fig. 11.13C, we can clearly see the coexistence of both

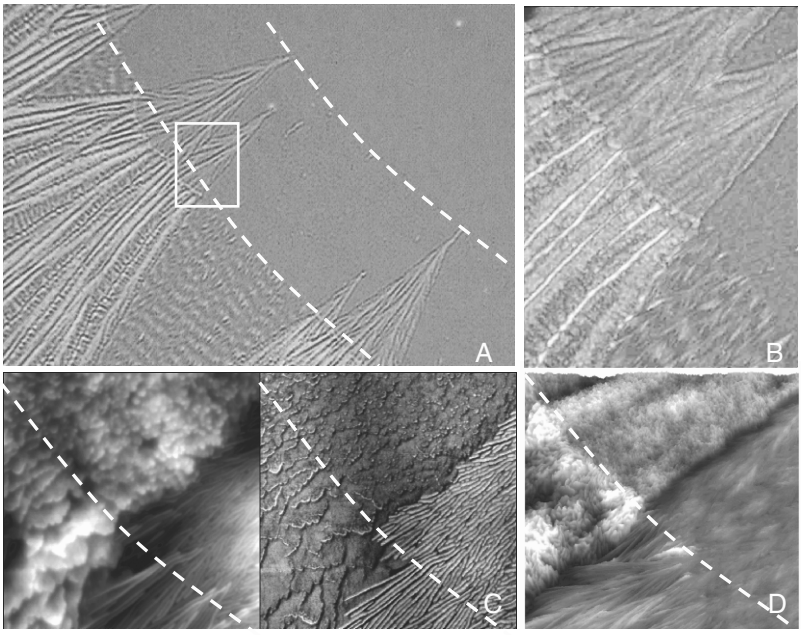

Fig. 11.13. Optical micrographs (A+B) and corresponding AFM images (C+D) showing that edge-on and flat-on lamellar structures can be formed simultaneously in a thin film. The temperature was raised in two steps from 40°C to 45°C and finally to 50°C. The film thickness is about 90 nm. The temperature transitions are indicated by broken lines. The lowest temperature is in the upper right corner of (**A**). Parts (**B**) and (**C**) represent the region selected by the white rectangle in A). In part C, both topography and phase image are shown. (**D**) is a 3D-representation of the transition zone between 40°C and 45°C. The size of the images is (A) $200 \times 140\ \mu m^2$, (B) $47 \times 63\ \mu m^2$, (C) $2 \times 2\ \mu m^2$, and (D) $10 \times 10\ \mu m^2$

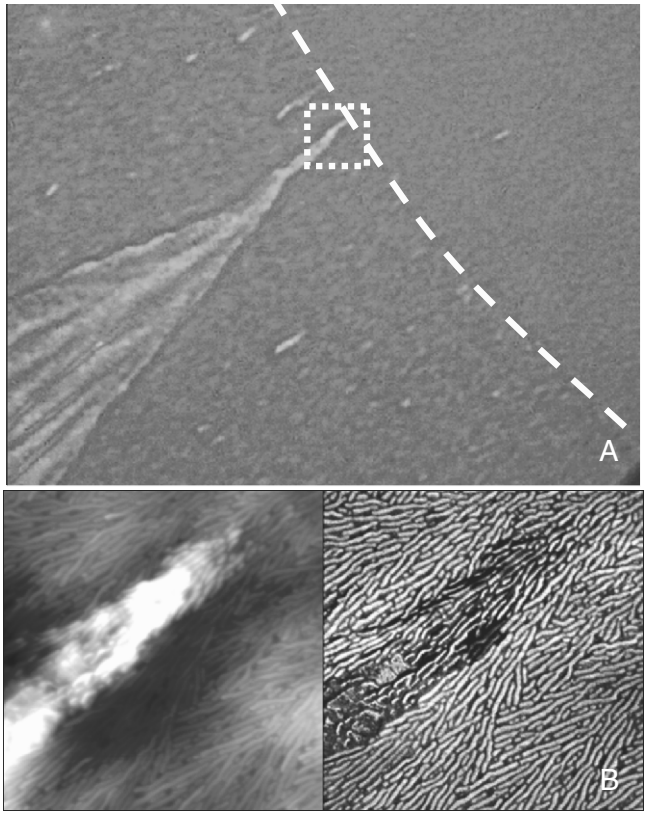

Fig. 11.14. (**A**) Optical micrograph (A) and (**B**) corresponding AFM image for the section indicated by the white square in (A) (including topography and phase information) showing the "birth" of a flat-on lamellar structure embedded within edge-on lamellae after the temperature was raised in a step (indicated by the *broken line*) from 40°C to 45°C. The film thickness is about 90 nm. The size of the images is (A) 63×47 μm^2, (B) 1.5×1.5 μm^2, height range: 40 nm

types of lamellae. It can also be seen that after increasing the temperature, the edge-on lamellae are more straight and the lateral size of the piled-up flat-on lamellae, probably formed by spirals resulting from screw dislocations, is larger. The more pronounced height variations seen in Fig. 11.13D indicate that the flat-on lamellae have the tendency to grow more in the direction normal to the substrate than the edge-on lamellae. The surface of flat-on lamellae is rougher than the edge-on counterparts. Thus, in interpreting optical microscopy images one has to take into account that more light is scattered on flat-on structures and that the edge-on lamellae appear smoother.

In Fig. 11.14 we can identify several attempts for the onset (nucleation) of flat-on lamellae. However, at the temperature of 45°C, even if nucleation

of flat-on structures does not seem to be the limiting step, only a few of these attempts finally grew further than a few micrometers. In our opinion, this indicates that the selection mechanism for the orientation is based on kinetics arguments. Only the fastest growing lamellae will "survive". Probably, in films thicker than one lamella, the orientation of polymer stems in the nuclei, which frequently form at the growth front, is not predetermined. In films thinner than one lamella, however, nucleation of edge-on lamellae may be more difficult than flat-on structures. However, if edge-on lamellae are somehow nucleated they may grow significantly faster.

11.4 Conclusions

The here presented examples of morphologies of lamellar polymer crystals strongly suggest that the concept of DLA is the most appropriate way of describing how these crystals have been formed. As this concept can be applied to most crystallising materials, we conclude that polymer crystallisation can be treated in such a unified way. It is not necessary to invoke special approaches to explain the various morphologies of polymer crystals.

Although we did not discuss the problem of nucleation in any depth, it is clear that, for the here studied system, it is extremely difficult to initiate crystallisation. Taking advantage of this difficulty allowed us to separate the nucleation step from the subsequent growth process and thus to analyse exclusively the growth kinetics of independent single crystals.

It is quite intriguing to observe that even the simple square-shaped crystals without any empty sites within their envelope seem to result from dendritic growth. There, the positions and the orientations of the square-shaped spirals decorating such "filled" crystals are indicating the growth pattern of the underlying first lamella. The orientation of the spirals is fully parallel to the orientation of the initial lamella. Moreover, these spirals are not distributed fully randomly on the surface. They are located along the supposed junction lines of the side-branches of the underlying dentrictic structure. Looking only at the square-shape envelope of such crystals, one may erroneously assume that they grew by attaching polymers to the sides. However, our results indicate that growth is dictated by the tips along the diagonals. One may distinguish several stages during the growth of such crystals. The crystals grow first along these diagonals. As a consequence of the diffusion limited transport process, side branches form in the direction orthogonal to the diagonals. Successive formation of more and more side branches, also of higher generations leads to the formation of the square shape envelope. At a length-scale much larger than the width of a single side-branch this envelope can be approximated quite well by straight lines.

Experiments with films of different thickness show that the quasi-two-dimensional growth morphologies are qualitatively the same, independent if more or less molecules than necessary for the formation of a single lamella are

available. The major difference of thicker films arises from the possibility to add polymers in between side branches by taking them from the "reservoir" on top of the lamella. This allows to close the gaps between side-branches. Our experiments indicate that this growth mode also favours the formation of spirals at the junctions between side-branches. One may speculate that the formation of such spirals, leading to stacked lamellae, is the major mode for growing the polymer crystals in three dimensions, even for single crystals.

The slow growth rates together with the possibility to form simple planar morphologies make polymer crystals ideal model systems for fundamental studies of crystal growth. Thus, combining these model experiments with theoretical concepts, including computer simulations, provides a highly promising approach for improving our understanding of polymer crystallisation and may also shed some light on central questions of crystal growth in general.

Acknowledgements

We are indebted to Dr. Cvetelin Vasilev for some preliminary experiments and to Bernard Lotz, Dimitri Ivanov, Gert Strobl, Wenbing Hu and Jens-Uwe Sommer for fruitful discussions. We acknowledge financial support provided through the the European Community's "Marie-Curie Actions" under contracts MRTN-CT-2003-505027 [POLYAMPHI] and MRTN-CT-2004-005516 [BioPolySurf].

References

[1] K. G. Libbrecht: Rep. Prog. Phys. **68**, 855 (2005).
[2] J. Langer: Rev. Mod. Phys. **52**, 1 (1980).
[3] P. Meakin, *Fractals, scaling and growth far from equilibrium*, Vol. 5 of *Cambridge Nonlinear Science Series*, Cambridge University Press, Cambridge (1998).
[4] E. Brener, H. Müller-Krumbhaar, D. Temkin: Phys. Rev. E, **54**, 2714 (1996).
[5] Y. Sakai, M. Imai, K. Kaji, M. Tsuji: J. Crystal Growth **203**, 244 (1999).
[6] G. Reiter, J.-U. Sommer: Phys. Rev. Lett. **80**, 3771 (1998).
[7] G. Reiter, J.-U. Sommer: J. Chem. Phys. **112**, 4376 (2000).
[8] J.-U. Sommer, G. Reiter: J. Chem. Phys. **112**, 4384 (2000).
[9] A. Holzwarth, S. Leporatti, H. Riegler: Europhys. Lett. **52**, 653 (2000).
[10] K. Taguchi, H. Miyaji, K. Izumi et al: Polymer **42**, 7443 (2001).
[11] K. Taguchi, H. Miyaji, K. Izumi et al: J. Macromol. Sci. B: Phys **41**, 1033 (2002).
[12] M.V. Massa, K. Dalnoki-Veress, J.A. Forrest: Eur. Phys. J. E **11**, 191 (2003).
[13] L. Granasy, T. Pusztai, T. Börzsönyi et al: Nat. Mat. **3**, 645 (2004).
[14] L. Granasy, T. Pusztai, G. Tegze et al: Phys. Rev. E **72**, 011605 (2005).
[15] K. Taguchi, Y. Miyamoto, H. Miyaji et al: Macromolecules **36**, 5208 (2003).
[16] G. Reiter, G. Castelein, J.-U. Sommer: Phys. Rev. Lett. **86**, 5918 (2001).

[17] J.-U. Sommer, G. Reiter: Europhys. Lett. **56**, 755 (2001).
[18] P. H. Geil, D. H. Reneker: J. Polym. Sci., **51**, 569 (1961).
[19] E.W. Fischer: Kolloid Z. u. Z. Polym., **231**, 458 (1968).
[20] A. Keller: Rep. Prog. Phys. **31**, 623 (1968).
[21] A. Kovacs, A. Gonthier, C. Straupe: J. Polym. Sci.: Polym. Symp. **50**, 283 (1975).
[22] A. Kovacs, C. Straupe, A. Gonthier: J. Polym. Sci.: Polym. Symp. **59**, 31 (1977).
[23] A.Kovacs, C. Straupe, J. Cryst. Growth: **48**, 210 (1980).
[24] G. Strobl: The Physics of Polymers, Springer, Berlin, Heidelberg, N.Y., 1997.
[25] A. Keller, S.Z.D. Cheng: Polymer **39**, 4461 (1998).
[26] K. Armistead and G. Goldbeck-Wood: Adv. Polym. Sci., **100**, 219 (1992).
[27] D. M. Sadler, G. H. Gilmer: Polymer **25**, 1446 (1984).
[28] H. D. Keith, F. J. Padden, Jr., B. Lotz et al: Macromolecules **22**, 2230 (1989).
[29] A. Toda, A. Keller: Colloid Polym. Sci. **271**, 328 (1993).
[30] S. Z. D. Cheng, B. Lotz: Polymer **46**, 8662 (2005)
[31] G. Strobl: Eur. Phys. J. E **18**, 295 (2005).
[32] B. Lotz, A.J. Kovacs: ACS Polym. Prepr. **10**, No. 2, 820 (1969).
[33] C. W. Frank, V. Rao, M. M. Despotopoulou et al: Science **273**, 912 (1996).
[34] G. Strobl, Eur. Phys. J. E: **3**, 165 (2000).
[35] G. Reiter, et al.: Phys. Rev. Lett. **83**, 3844 (1999).
[36] A. Winkel, J. Hobbs, M. Miles: Polymer **41**, 8791 (2000).
[37] C. Basire, D.A. Ivanov: Phys. Rev. Lett. **85**, 5587 (2000).
[38] Y.K. Godovsky, S. Magonov: Langmuir **16**, 3549 (2000).
[39] L. Li, C.-M. Chan, K.L. Yeung: J.-X. Li, K.-M. Ng, Y. Lei, Macromolecules **34**, 316 (2001).
[40] Y.-L. Loo, R.A. Register, A.J. Ryan: Phys. Rev. Lett. **84**, 4120 (2000).
[41] C. De Rosa, C. Park, E.L. Thomas, B. Lotz: Nature **405**, 433 (2000).
[42] G. Reiter, G. Castelein, J.-U. Sommer, A. Röttele, T. Thurn-Albrecht: Phys. Rev. Lett. **87**, 226101 (2001).
[43] P. N. Chaturvedi: J. Mater. Sci. **29**, 3749 (1994).
[44] C. Liu, M. Muthukumar: J. Chem. Phys. **109**, 2536 (1998).
[45] P.D. Olmsted et al.: Phys. Rev. Lett. **81**, 373 (1998).
[46] W. Zhou et al.: Macromolecules **33**, 6861 (2000).
[47] M. Psarski, E. Piorkowska, A. Galeski: Macromolecules **33**, 916 (2000).
[48] F. Zhang, J. Liu, H. Huang et al: Eur. Phys. J. E **8**, 289 (2002).
[49] Y. Kikkawa, H. Abe, T. Iwata et al : Biomacromolecules **3**, 350 (2002).
[50] Y. Kikkawa, H. Abe, M. Fujita et al: Macromol. Chem. Phys. **204**, 1822 (2003).
[51] M. Wang, H.-G. Braun, E. Meyer: Polymer **44**, 5015 (2003).
[52] E.-Q. Chen, A. J. Jing, X. Wenig et al: Polymer **44**, 6051 (2003).
[53] R. Kurimoto, A. Kawaguchi: J. Macromol. Sci. B: Phys **42**, 441 (2003).
[54] Y.-G. Lei, C.-M. Chan, Y. Wang et al: Polymer **44**, 4673 (2003).
[55] R. Mehta, W. Keawwattana, A. L. Guenthner et al: Phys. Rev. E **69**, 061802 (2004).
[56] M. Tian, M. Dosiere, S. Hocquet et al: Macromolecules **37**, 1333 (2004).
[57] A. Tracz, I. Kucinska, J. K. Jeszka: Macromolecules **36**, 10130 (2003).
[58] N. Dubreuil, S. Hocquet, M. Dosière et al: Macromolecules **37** (1), 1 (2004).
[59] M. V. Massa, K. Dalnoki-Veress: Phys. Rev. Lett. **92**, 255509 (2004).
[60] Y. Wang, S. Ge, M. Rafailovich et al: Macromolecules **37**, 3319 (2004).
[61] A. Toda, M. Okamura, M. Hikosaka et al: Polymer **46**, 8708 (2005).

[62] C. Qiao, J. Zhao, S. Jiang et al: J. Polym. Sci., Part B: Polym. Phys. **43**, 1303 (2005).
[63] X.-M. Zhai, W. Wang, Z.-P. Ma et al : Macromolecules **38**, 1717 (2005).
[64] H. Xu, R. Matkar, T. Kyu: Phys. Rev. E **72**, 011804 (2005).
[65] V. H. Mareau, R. E. Prud'homme: Macromolecules **38**, 398 (2005).